ELSEVIER

Thermochimica Acta 293 (1997) 65–76

thermochimica acta

Thermal decomposition of cerous ammonium nitrate tetrahydrate studied with temperature-dependent X-ray powder diffraction and thermal analysis

Nathalie Audebrand, Jean-Paul Auffrédic, Daniel Louër*

Laboratoire de Chimie du Solide, et Inorganique Moleculaire, (UMR 6511 CNRS), Groupe de Cristallochimie, Université de Rennes, Avenue du Général Leclerc, 35042-Rennes cedex, France

Received 12 July 1996

Abstract

The thermal decomposition process of $Ce(NH_4)_2(NO_3)_5.4H_2O$ has been determined by means of temperature-dependent X-ray diffraction and TG–DSC. The transformations are particle-size dependent and have been studied in nitrogen and vacuum. The occurrence of $Ce(NH_4)_2(NO_3)_5.3H_2O$, $Ce(NH_4)_2(NO_3)_5.2H_2O$, $Ce(NH_4)_2(NO_3)_5$, $Ce_2(NH_4)_3(NO_3)_9$ or a mixture of these last two phases, as well as the formation of amorphous NH_4NO_3 have been demonstrated. The diffraction powder patterns have been indexed, a linear variation of the chemical-formula-unit equivalent volumes V_{eq} with the number of water molecules has been derived from the unit-cell volumes. © 1997 Elsevier Science B.V.

Keywords: Amorphous ammonium nitrate; Cerous ammonium nitrate tetrahydrate- $Ce(NH_4)_2(NO_3)_5.4H_2O$; Temperature-dependent X-ray powder diffraction (TDXD); TG–DSC; Thermal decomposition

1. Introduction

In the recent years, we have thoroughly investigated the thermal decomposition of a number of mixed cerium nitrates with a monovalent cation. For the cerium (IV) phases, $Ce^{IV}M^{I}_2(NO_3)_6$(M = NH_4, K, *Rb*) [1–3], a noteworthy double change of the valence of cerium was described and increasingly complex decomposition mechanisms were observed according to the sequence order NH_4, K, Rb. To explain the reaction schemes it has been necessary to study the structural properties and thermal behaviour of the related cerium (III) phases, i.e. $Ce_2K_3(NO_3)_9$ [4], $Ce_2Rb_3(NO_3)_9$ [3] and $CeRb_2(NO_3)_5.4H_2O$ [5]. For the last two compounds, though the decomposition processes were complex, it was clearly demonstrated that amorphous rubidium nitrate was formed during the decomposition, before its sudden crystallization at higher temperature. It is a surprising feature and, consequently, it is of interest to know if a similar behaviour is observed in the related cerium (III) ammonium system, for which a simpler thermal decomposition can be expected. On the other hand, the formation of ammonium nitrate as an intermediate phase on heating is questionable, since it is known as thermodynamically unstable at temperatures close to its melting point.

Solid pentanitrato-complexes of rare earths of general formula $LnM_2(NO_3)_5.nH_2O$ (M^1=alkaline or ammonium ion, Ln=lanthanide) have been extensively studied (see, for example, [6]). Decomposition

*Tel.: 0033-29928-6248; Fax: 0033-29938-3487

PII S0040-6031(97)00064-6

schemes for the ammonium compounds with Ln= La, Pr and Nd have been already reported [7,8]. The successive intermediate phases preceding the formation of Ln_2O_3, reported from thermogravimetry measurements (TG), were $Ln(NH_4)_2(NO_3)_5.2H_2O$, $Ln(NH_4)_2(NO_3)_5$, $Ln_2(NH_4)_3(NO_3)_9$, $Ln(NO_3)_3$ and $LnONO_3$. In the case of the praseodymium compound the formation of $Pr(NH_4)(NO_3)_4$ was also proposed [8].

The present study deals with the synthesis and the thermal behaviour of the cerium (III) ammonium nitrate $Ce(NH_4)_2(NO_3)_5.4H_2O$. Its thermal decomposition is investigated with Temperature-Dependent X-ray powder Diffraction (TDXD), TG and differential scanning calorimetry (DSC). A special attention is paid to the environmental atmosphere and to the particle size of the precursor. In addition, structural features are described for some intermediate phases.

2. Experimental

2.1. Material preparation

The new compound $Ce(NH_4)_2(NO_3)_5.4H_2O$ was synthesized from a solution of cerous nitrate and ammonium nitrate. A mixture of analytical grade $Ce(NO_3)_3.6H_2O$ (Prolabo) and NH_4NO_3 (Prolabo), with a stoichiometric 1 : 2 ratio (Ce : NH_4), was heated at 30°C to obtain a liquid phase, to which 2 ml of water were added. Colourless crystals were grown from this solution, at 40°C, after about 10 days.

For thermal and X-ray diffraction studies, the samples were ground manually or in cyclohexane, using a micronizing mill from McCrone Research. An estimation of particle size was carried out from optical microscopy measurements. For the two samples studied, the average sizes were found to be higher than 50 μm and lower than 13 μm, respectively.

2.2. X-ray powder diffraction

X-ray powder diffraction data were collected by means of a high-resolution powder diffractometer (Siemens 0500) with an incident-beam monochromator ($CuK\alpha_1$ radiation, λ=1.5406 Å), for ex situ measurements at room temperature, and a diffractometer (Siemens) with a diffracted-beam monochromator ($CuK\alpha_{1,2}$ radiation), equipped with a furnace, for in situ measurements. To prevent the hydration of the compounds studied ex situ, the samples were kept in a nitrogen atmosphere by using a tight sample holder. Patterns were scanned with a step length of 0.02°(2θ). The peak positions were extracted by the pattern decomposition technique using the fitting program PROFILE from Socabim, available in the software package DIFFRAC-AT supplied by Siemens. Indexing of the powder patterns was performed with the program DICVOL91 [9].

TDXD experiments were carried out with an INEL (CPS120) curved-position-sensitive detector, used in a diffraction geometry by reflection ($CuK\alpha_1$) described elsewhere [10]. The stationary sample was heated in a monitored high-temperature device (Rigaku), in flowing air or nitrogen (40 ml min^{-1}) or in vacuum (10^{-2} Torr). In order to ensure satisfactory counting statistics a counting time of 2500 s per pattern was selected. The 3-dimensional TDXD plots displaying the changes in the powder diffraction patterns with time or temperature were performed with a Socabim software.

2.3. Thermogravimetry and differential scanning calorimetry

Simultaneous TG–DSC measurements were carried out in a stream of air or nitrogen (40 ml min^{-1}) using a Thermoflex TG–DSC instrument (Rigaku) with a sample mass between 10 and 20 mg. When only the TG curve was recorded, a sample mass between 50 and 100 mg was spread evenly in a large sample holder to avoid mass effects and to reproduce as much as possible the experimental conditions used in TDXD. TG analyses under vacuum, or under a selected water-vapour pressure, were carried out using a thermobalance of McBain type with a sample mass of about 50 mg spread in a thin layer. The vessel was evacuated (< 10^{-2} Torr) before admitting the stream of nitrogen or the constant water-vapour pressure, which was generated from a bulb containing a sulfuric acid solution maintained at a constant temperature. The water-vapour pressure was calculated from data reported by Boll [11].

3. Results and discussion

3.1. Powder pattern indexing of the precursor

A monoclinic unit cell was proposed by DICVOL91. The cell parameters were used for reviewing the complete powder data by means of the evaluation program NBS*AIDS83 [12]. The refined parameters were $a = 11.090(1)$ Å, $b = 8.934(1)$ Å, $c = 17.927(2)$ Å, $\beta = 101.75(1)°$, $V = 1738.9(2)$ Å^3 [$M_{20} = 45$, $F_{30} = 114(0.0069, 38)$]. (The powder data have been deposited with the ICDD [13].) It is interesting to note the analogy with the cell parameters of $La(NH_4)_2(NO_3)_5.4H_2O$ [$a = 11.152(5)$ Å, $b = 8.966(4)$ Å, $c = 17.881(6)$ Å, $\beta = 101.6(4)°$] [14], and those of $CeRb_2(NO_3)_5.4H_2O$ [$a = 11.050(1)$ Å, $b = 8.977(1)$ Å, $c = 17.859(2)$ Å, $\beta = 100.877(9)°$] [5]. Consequently, these compounds are isostructural, with the space group Cc, as demonstrated recently by the structure determination of $CeRb_2(NO_3)_5.4H_2O$ [5]. The structure of $Ce(NH_4)_2(NO_3)_5.4H_2O$ can then be described as built from $[Ce(NO_3)_5.(H_2O)_2]^{2-}$ ions in the form of irregular icosahedra. These polyhedra are independent and connected through hydrogen bonds. Ammonium ions and 'free' water molecules are located between the polyhedra and develop chains parallel to [010], with the sequence H_2O–NH_4–H_2O–NH_4.

3.2. Decomposition scheme of $Ce(NH_4)_2(NO_3)_5.4H_2O$

The thermal decomposition scheme of $Ce(NH_4)_2(NO_3)_5.4H_2O$ depends on the environmental atmosphere and on the particle size of the sample. The results obtained for the decompositions carried out in flowing nitrogen, or in vacuum, with samples of particle size greater than 50 μm or lower than 13 μm are described.

3.2.1. Thermal decomposition in nitrogen.

Figs. 1 and 2 display two representative 3-dimensional plots of the evolution of the powder diffraction patterns obtained from a precursor with particle size lower than 13 μm. Fig. 3 is ascribed to a precursor with particle size greater than 50 μm. The weight loss at room temperature is shown in Fig. 4 and the TG experiment is displayed in Fig. 5 for the two samples. This TG study suggests that the decomposition proceeds through four stages and shows that a decrease of

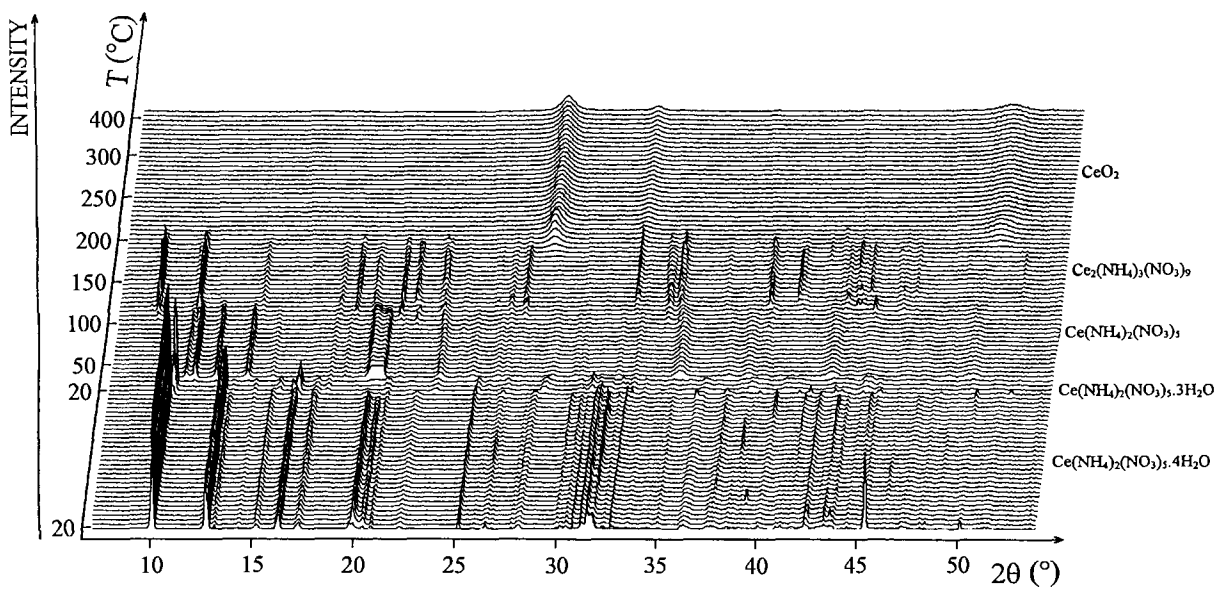

Fig. 1. TDXD plot for $Ce(NH_4)_2(NO_3)_5.4H_2O$ (particle size < 13 μm), in nitrogen (20 h at 20°C, 8°C h^{-1} in the range 20–320°C, 25°C h^{-1} in the range 320–500°C).

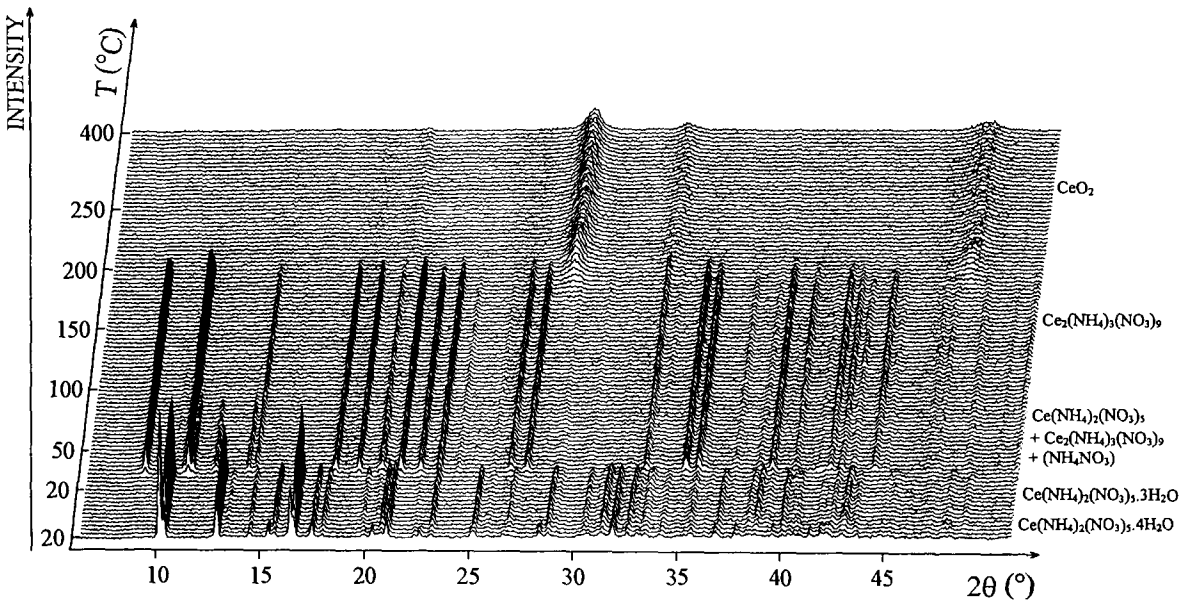

Fig. 2. TDXD plot for $Ce(NH_4)_2(NO_3)_5.4H_2O$ (Particle size < 13 μm), in nitrogen (10 h at 20°C, 5°C h^{-1} in the range 20-300°C, 40°C h^{-1} in the range 300–400°C). '(NH_4NO_3)' means that the solid is amorphous.

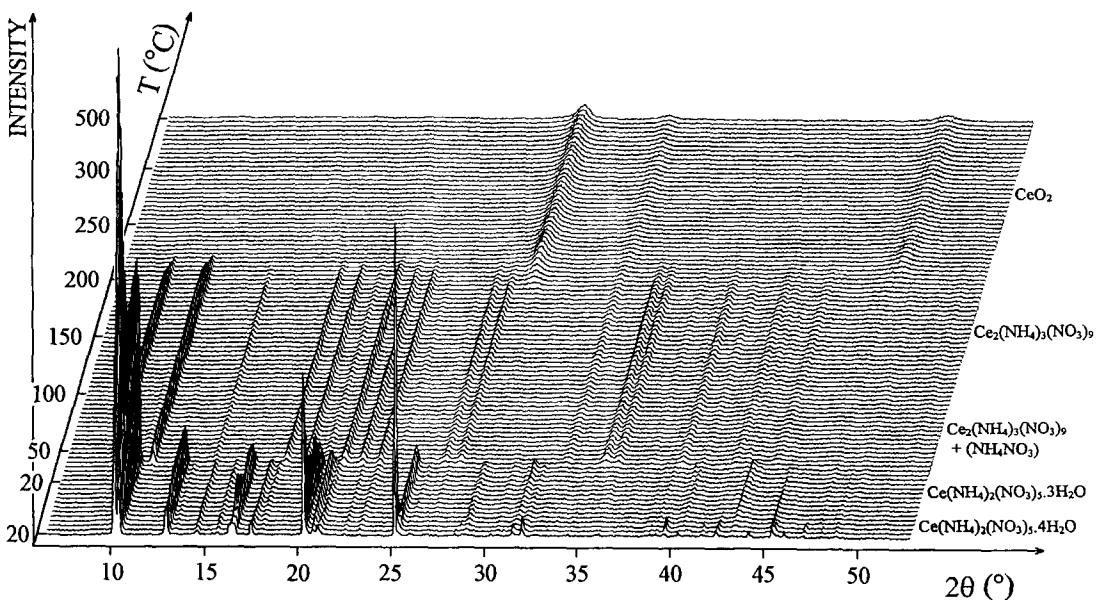

Fig. 3. TDXD plot for $Ce(NH_4)_2(NO_3)_5.4H_2O$ (Particle size > 50 μm), in nitrogen (9 h at 20°C, 6°C h^{-1} in the range 20–300°C, 30°C h^{-1} in the range 300–500°C). '(NH_4NO_3)' means that the solid is amorphous.

the grain size of the precursor enhances the kinetic of the successive transformations, as expected (see curves a and b in Fig. 4 and Fig. 5). On the other hand, three or four stages can be deduced from TDXD.

At room temperature (Fig. 2 and Fig. 3), after a short time in nitrogen atmosphere, the precursor gives a new compound whose diffraction pattern was found similar to that of $CeRb_2(NO_3)_5.3H_2O$ [5]. Further-

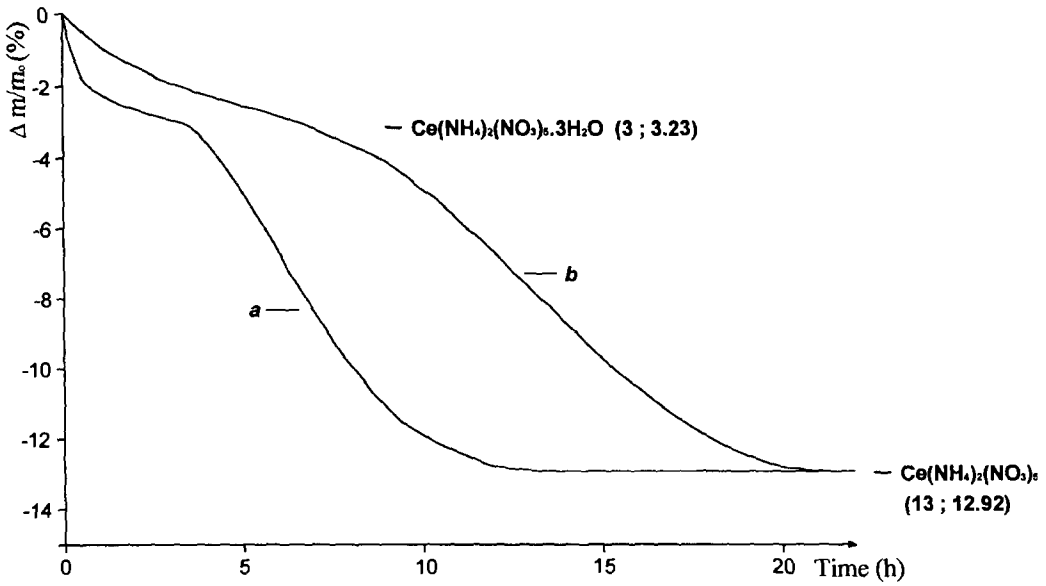

Fig. 4. TG curves for the decomposition, in nitrogen, of $Ce(NH_4)_2(NO_3)_5.4H_2O$ versus time, at room temperature. (a) particle size < 13 μm, (b) particle size > 50 μm. Experimental and theoretical weight losses (%) are given in parentheses, respectively.

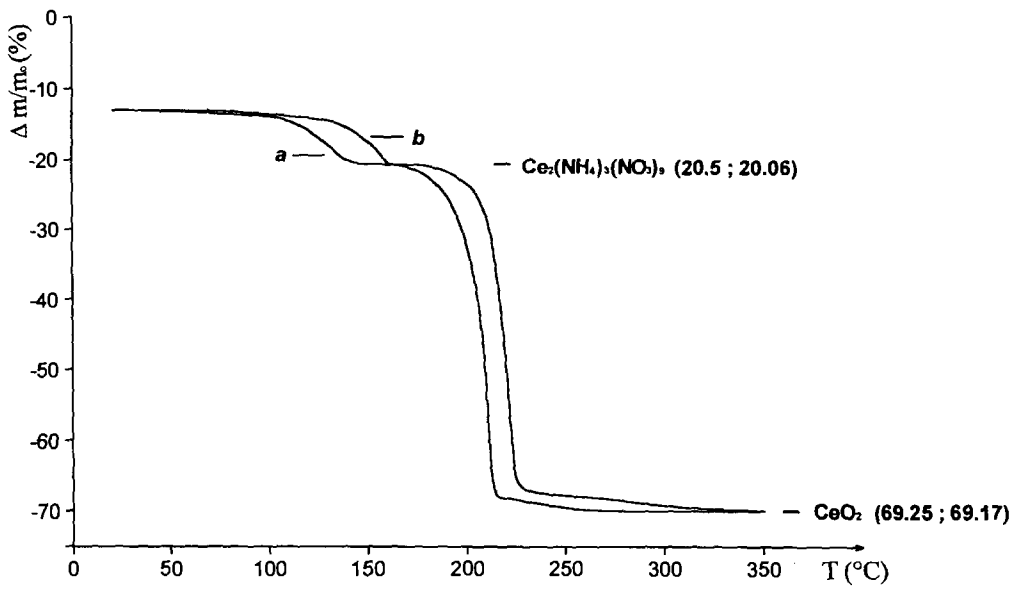

Fig. 5. TG curves for the decomposition of $Ce(NH_4)_2(NO_3)_5.4H_2O$ in nitrogen. (a) 5°C h^{-1}, particle size < 13 μm, (b) 6°C h^{-1}, particle size > 50 μm. Experimental and theoretical weight losses (%) are given in parentheses, respectively.

more, the TG curves (Fig. 4, curves a and b) present an inflection point where the weight loss agrees well with the departure of one water molecule (experimental: ~3%; theoretical: 3.23%). Consequently, the formation of $Ce(NH_4)_2(NO_3)_5.3H_2O$ can be stated in the first stage. Nevertheless, in some cases, as seen in Fig. 1, the structural transformation of the precursor is delayed with regard to the weight loss and occurs

only on heating. Such a non-synchronism between structural transformation and weight loss has already been reported [5]. This change in reactivity of the precursor is likely to be related with the microstructural properties of the samples (crystallite sizes and/or strain effects), which cannot be quantified.

In the second stage, while the weight loss observed at room temperature (Fig. 4) displays a plateau corresponding to a global chemical formula $Ce(NH_4)_2(NO_3)_5$ (experimental: 13%; theoretical: 12.92%), the TDXD experiments show that the transformation of the trihydrated phase occurs only above 40°C approximately (Fig. 1, Fig. 2, Fig. 3). Nevertheless, the products of this transformation are dependent on the precursor-grain size. For sizes lower than 13 μm, either a new compound, with a diffraction pattern similar to that of α-$CeRb_2(NO_3)_5$ [5] (Fig. 1), or a mixture of this new phase and $Ce_2(NH_4)_3(NO_3)_9$ [1] is obtained (Fig. 2). For sizes greater than 50 μm, the formation of $Ce_2(NH_4)_3(NO_3)_9$ is only observed (Fig. 3). To explain these results, and taking into account the possibility of the formation of amorphous neutral nitrate as observed in the study of related rubidium compounds [3,5], three alternative interpretations based on the same global chemical weight loss must be suggested:

1. the formation of $Ce(NH_4)_2(NO_3)_5$, as observed in Fig. 1,
2. the simultaneous formation of NH_4NO_3 and $Ce_2(NH_4)_3(NO_3)_9$ (Fig. 3),
3. or the superposition of (1) and (2) (Fig. 2).

Nevertheless, it must be noted that NH_4NO_3 is not observed in the diffraction patterns recorded during this stage (Fig. 2 and Fig. 3). Consequently, the last two alternatives are only plausible if NH_4NO_3 is in an amorphous state, similarly to the rubidium nitrate observed in the decomposition of $Ce_2Rb_3(NO_3)_9$ [3] and $CeRb_2(NO_3)_5.4H_2O$ [5]. In order to demonstrate the formation of amorphous NH_4NO_3 a simultaneous TG–DSC experiment was carried out by using a heating rate of 20°C h^{-1}. As shown in Fig. 6, two endothermic events take place simultaneously between 150 and 190°C. The first one is broad and corresponds to a decomposition process. The second peak is sharper and occurs in the range 166–171°C. It corresponds to the melting of pure NH_4NO_3, which

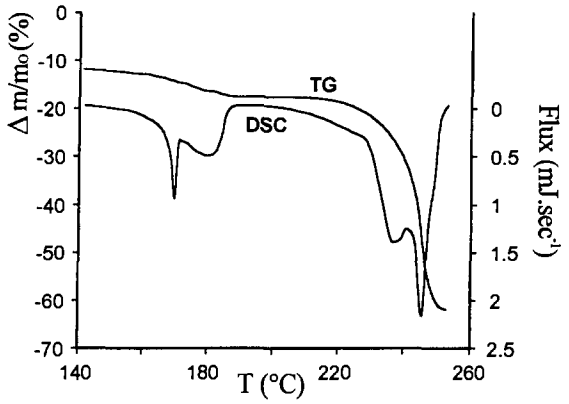

Fig. 6. TG and DSC curves for the decomposition of $Ce(NH_4)_2(NO_3)_5.4H_2O$, in nitrogen. 20°C h^{-1}, particle size > 50 μm.

occurs at 170°C [15], as shown from a complementary DSC experiment. Consequently, this feature demonstrates that ammonium nitrate is necessarily formed in the second stage of the decomposition, simultaneously with $Ce_2(NH_4)_3(NO_3)_9$. However, the amount of NH_4NO_3 formed at this stage could not be calculated since its heat of fusion is not known with accuracy, a consequence of a partial decomposition of the solid occurring during melting.

In the third stage, the experimental weight loss is 20.5% and the product obtained is $Ce_2(NH_4)_3(NO_3)_9$, as shown by the TDXD plots (Fig. 1, Fig. 2, Fig. 3). Consequently, this stage corresponds either to the total transformation of $Ce(NH_4)_2(NO_3)_5$ (Fig. 1), or to the transformation of the mixture of $Ce(NH_4)_2(NO_3)_5$–NH_4NO_3 (Fig. 2), or to the decomposition of NH_4NO_3 (Fig. 3) (theoretical weight loss for the three alternatives: 20.06%). The last case is supported by the fact that the intensity of the diffraction lines of $Ce_2(NH_4)_3(NO_3)_9$ remains constant over the temperature range 45–195°C. On the other hand, amorphous NH_4NO_3 decomposes totally before its melting point (see Fig. 5), which is due to the low heating rate (5–8°C h^{-1}) used in TDXD and TG, with respect to the conditions used in the DSC experiment (20°C h^{-1}). The third stage is followed by the rapid transformation of $Ce_2(NH_4)_3(NO_3)_9$ into CeO_2, while the total desorption of the gaseous products from the nanocrystalline oxide is achieved at about 350°C (Fig. 5).

Table 1 summarizes the successive reaction stages together with their weight losses and temperature ranges, obtained from TDXD or TG for the two

Table 1
Reactions stages with weight losses and temperature ranges from TDXD and TG in nitrogen for $Ce(NH_4)_2(NO_3)_5.4H_2O$.

Particle size (μm)	Stage	Transformation	Total weight loss (%) observed/ calculated	Temperature range (°C) TDXD/TG
< 13	1	$Ce(NH_4)_2(NO_3)_5.4H_2O \rightarrow Ce(NH_4)_2(NO_3)_5.3H_2O + H_2O \nearrow$	3/3.23	RT[b]
	2	$Ce(NH_4)_2(NO_3)_5.3H_2O \rightarrow Ce(NH_4)_2(NO_3)_5 + 3H_2O \nearrow$ or $Ce(NH_4)_2(NO_3)_5.3H_2O \rightarrow x\,Ce(NH_4)_2(NO_3)_5 + \frac{1-x}{2}Ce_2(NH_4)_3(NO_3)_9 + \frac{1-x}{2}NH_4NO_3^a + 3H_2O \nearrow$	13/12.92	36–40/RT[b]
	3	$Ce(NH_4)_2(NO_3)_5 \rightarrow 1/2Ce_2(NH_4)_3(NO_3)_9 + (NH_3, NO, NO_2, O_2) \nearrow$ or $x\,Ce(NH_4)_2(NO_3)_5 + \frac{1-x}{2}NH_4NO_3^a \rightarrow \frac{x}{2}Ce_2(NH_4)_3(NO_3)_9 + (NH_3, NO, NO_2, O_2) \nearrow$	20.5/20.06	115–140/85–140 or 85–115/85–140
	4	$1/2Ce(NH_4)_3(NO_3)_9 \rightarrow CeO_2 + (NH_3, NO, NO_2, O_2) \nearrow$	70/69.7	185–215/175–300
> 50	1	$Ce(NH_4)_2(NO_3)_5.4H_2O \rightarrow Ce(NH_4)_2(NO_3)_5.3H_2O + H_2O \nearrow$	3/3.23	RT[b]
	2	$Ce(NH_4)_2(NO_3)_5.3H_2O \rightarrow 1/2\,Ce_2(NH_4)_3(NO_3)_9 + 1/2NH_4NO_3^a + 3H_2O \nearrow$	13/12.92	37–45/RT[b]
	3	$1/2NH_4NO_3^a \rightarrow (NH_3, NO, NO_2, O_2) \nearrow$	20.5/20.06	–/90–160
	4	$1/2Ce_2(NH_4)_3(NO_3)_9 \rightarrow CeO_2 + (NH_3, NO, NO_2, O_2) \nearrow$	69.5/69.17	195–220/180–500

[a] amorphous state,
[b] RT: room temperature, 0<x<1.

samples of the precursor with different particle size. It has been verified that similar schemes are valid when the thermal decomposition is carried out in air.

3.2.2. *Thermal decomposition in vacuum*

From Figs. 7–10, the main features of the thermal decomposition performed in vacuum, for samples with the two different particle sizes, can be described as follows:

1. The dehydration of $Ce(NH_4)_2(NO_3)_5.4H_2O$ occurs immediately at room temperature, giving successively the trihydrated phase and a new compound (Fig. 7 and Fig. 8), whose diffraction pattern presents analogies with that of $CeRb_2(NO_3)_5.2H_2O$ [5], and finally the anhydrous phase. The inflection point observed on the TG curve (Fig. 9, curve *a*, weight loss: ~7.1%), suggests that two water molecules are released from the precursor (theoretical weight loss: 6.46%)and, then, that $Ce(NH_4)_2(NO_3)_5.2H_2O$ is formed. Its existence was confirmed by a TG curve, obtained at 13°C under a water pressure of 0.05 Torr, which displayed a stable plateau with a weight loss of 6.52% (Fig. 9, curve c). The diffraction pattern of the dihydrated phase was observed for about 7 h, while the composition of the solid, deduced from TG, corresponds to the anhydrous phase (Fig. 9, curves a and b). Similar features have been already commented above and elsewhere [5].
2. As a consequence of the different microstructural properties of the two samples of precursor, the anhydrous phase is obtained in a crystalline form (Fig. 8) or in an amorphous or highly divided state (Fig. 7). Subsequently, it either gives a well or poorly crystallized $Ce_2(NH_4)_3(NO_3)_9$, respectively. Also, as shown by the TG curves (Fig. 9 and Fig. 10, curves a and b), the microstructure of the precursor greatly influences the kinetic of the weight loss.
3. The decomposition of $Ce_2(NH_4)_3(NO_3)_9$ leads to CeO_2 in the last stage. It can be seen that the diffraction lines of CeO_2 are very broad, which indicates that this oxide is nanocrystalline.

These results demonstrate that the decomposition in vacuum proceeds through the successive formation of $Ce(NH_4)_2(NO_3)_5.3H_2O$, $Ce(NH_4)_2(NO_3)_5.2H_2O$, $Ce(NH_4)_2(NO_3)_5$, $Ce_2(NH_4)_3(NO_3)_9$ and, finally, CeO_2.

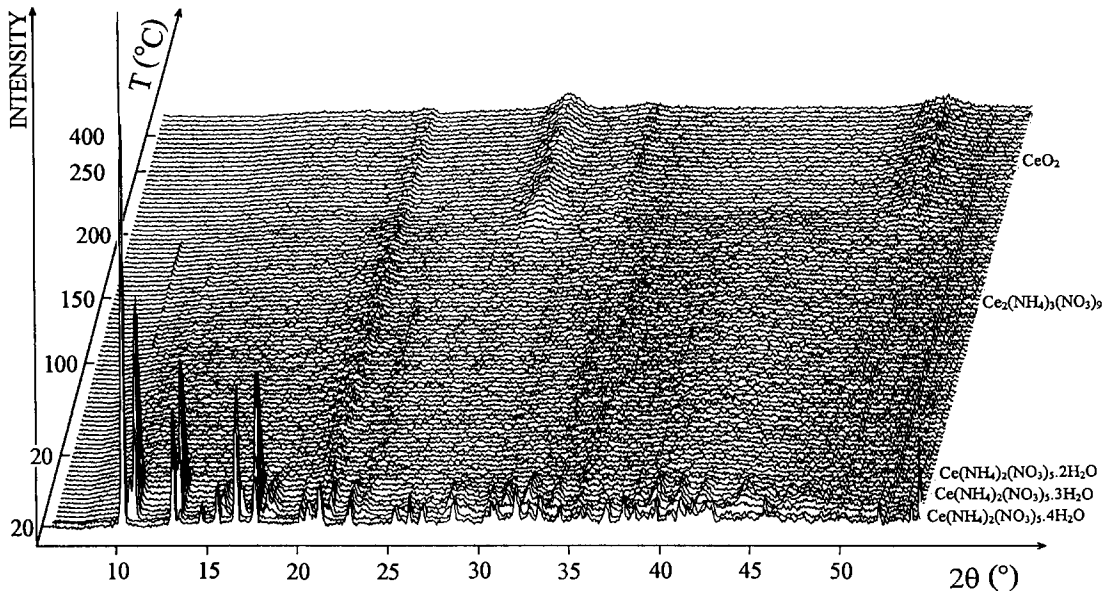

Fig. 7. TDXD plot for $Ce(NH_4)_2(NO_3)_5.4H_2O$ (particle size < 13 μm), in vacuum (11 h at 20°C, 5°C h^{-1} in the range 20–250°C, 30°C h^{-1} in the range 250–500°C). The first powder diffraction pattern was recorded in air.

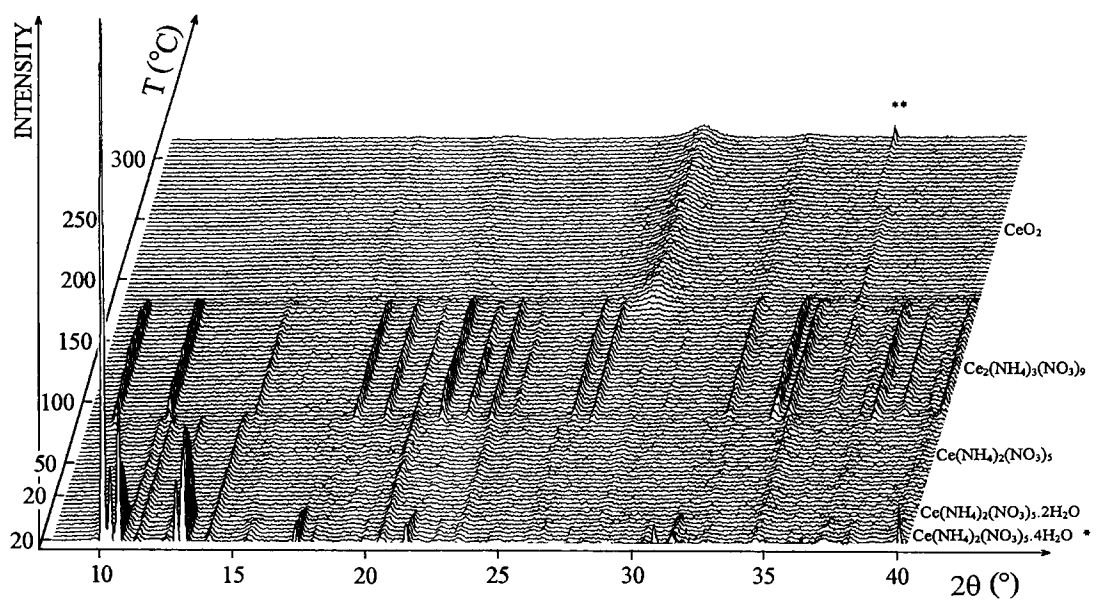

Fig. 8. TDXD plot for $Ce(NH_4)_2(NO_3)_5.4H_2O$ (Particle size > 50 μm), in vacuum (8 h at 20°C, 5°C h^{-1} in the range 20–300°C, 30°C h^{-1} in the range 300–400°C). (*) mixture of tetra- and trihydrated phase, (**) spurious lines due to the sample holder.

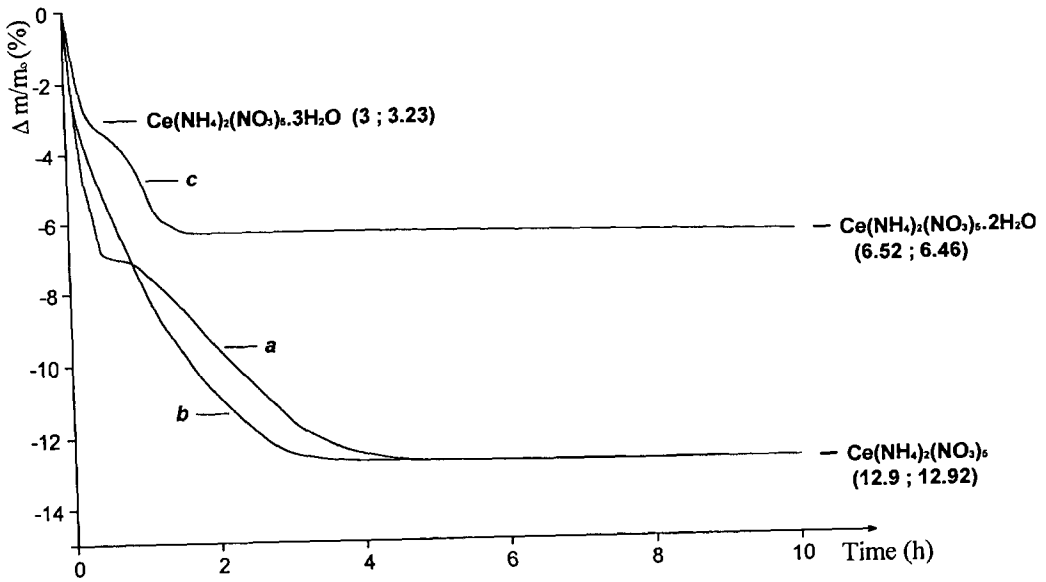

Fig. 9. TG curves for the decomposition of $Ce(NH_4)_2(NO_3)_5.4H_2O$ versus time. (a) in vacuum at 20°C, particle size < 13 μm, (b) in vacuum at 20°C, particle size > 50 μm, (c) in reduced water-vapour pressure (0.05 Torr) at 13°C, particle size < 13 μm. Experimental and theoretical weight losses (%) are given in parentheses, respectively.

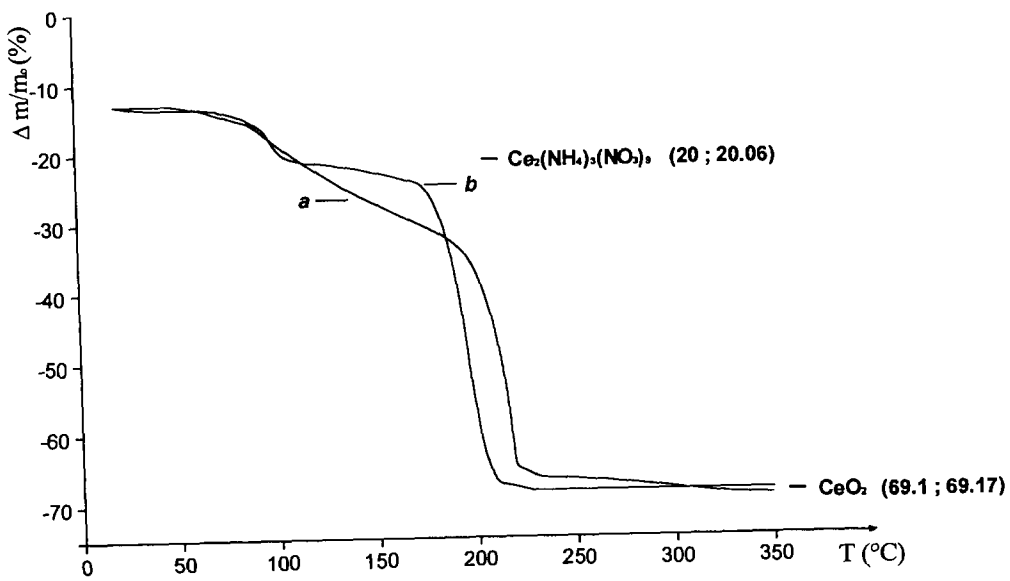

Fig. 10. TG curves for the decomposition of $Ce(NH_4)_2(NO_3)_5.4H_2O$, in vacuum, at 7°C h^{-1}. (a) particle size < 13 μm, (b) particle size 50 μm. Experimental and theoretical weight losses (%) are given in parentheses, respectively.

3.3. Characterization of the intermediate phases

The intermediate phases $Ce(NH_4)_2(NO_3)_5.3H_2O$, $Ce(NH_4)_2(NO_3)_5.2H_2O$ and $Ce(NH_4)_2(NO_3)_5$ have been characterized by X-ray diffraction.

1. $Ce(NH_4)_2(NO_3)_5.3H_2O$– The diffraction pattern (data collected in situ, under nitrogen, 17°C) was indexed with a monoclinic unit cell, the refined parameters are: a = 10.869(2) Å, b = 8.980(2) Å, c = 17.345(4) Å, β = 100.15(2)°, V = 1666.3(4) Å^3 [M_{20} = 40, F_{30} = 67(0.0079, 57)]. (The powder data have been deposited with the ICDD [13].) It is interesting to note the apparent relationships of this solution with the unit cell parameters of the related phases $La(NH_4)_2(NO_3)_5.3H_2O$ [a = 10.969(10) Å, b=9.012(5) Å, c=17.439(10) Å, β= 100.1(1) Å] [14] and $CeRb_2(NO_3)_5.3H_2O$ [a=10.850(5) Å, b = 9.046(3) Å, c = 17.402(6) Å, β = 100.47(3)°, Z = 4, space group Cc] [5], which suggests the existence of isostructural properties. Moreover, the parameters also present analogies with those found for the precursor (see Section 3.1). Consequently, the structure of this trihydrated phase should be derived from that of the precursor by removing half of the two 'free' water molecules, as already discussed for the related rubidium compound [5].
2. $Ce(NH_4)_2(NO_3)_5.2H_2O$– In spite of significant line broadening the diffraction pattern (data collected in situ, under vacuum, 13°C) was indexed with a monoclinic unit cell, the refined parameters are: a = 10.604(4) Å, b = 9.005(3) Å, c = 17.191(4) Å, β = 104.61(2)°, V = 1588.5(6) Å^3 [M_{20} =14, F_{30} = 25 (0.0113, 108)]. (The powder data have been deposited with the ICDD [13]). The figures of merit are low, due to the poor quality of the data, however the discussion below (see, also, Fig. 11) indicates the relevance of the solution. The unit cell parameters again present analogies with those of the two higher hydrates, an indication about probable structural relationships, based on the elimination of the 'free' water molecules in the tetrahydrated compound.
3. $Ce(NH_4)_2(NO_3)_5$– The diffraction pattern (data collected ex situ, under nitrogen) was indexed with an orthorhombic unit cell, the refined parameters are: a = 18.444(1) Å, b = 17.499(1) Å, c = 8.6514(5) Å, V = 2792.2(2) Å^3 [M_{20} = 56, F_{30} = 108 (0.0048, 57)]. (The powder data have been deposited with the ICDD [13]). This solution compares well with the orthorhombic unit cell parameters found for α-$CeRb_2(NO_3)_5$ [a = 18.228(7) Å, b = 17.492(6) Å, c = 8.797(4) Å, V = 2805.0 Å^3] [5]. It can be seen that there is no evident cell parameter analogies with those of the hydrated phases. Therefore, a different structural organization should be stated, as expected from the departure of the two water molecules contributing to the cerium polyhedra in the structure of the precursor. Although the structure could not be solved entirely from powder diffraction data, some features deserve to be mentioned. Integrated intensities were extracted using the pattern matching option available in the Rietveld refinement program FULLPROF [16]. They were used as input data in the program SHELXS-86 [17], assuming space group $P2_12_12_1$ (Z = 8). The calculation of a 3-dimensional Patterson function yielded vectors consistent with the location of two cerium atoms. The refinement of these positions led to residual factor R_F = 0.22. Subsequent Fourier difference analyses did not allow to determine the positions of the remaining atoms. However, from this study, it can be suggested that the structure is built from infinite zigzag chains of $[Ce(NO_3)_5^{2-}]$n groups running along [010]. The Ce–Ce distance close to 5.4 Å is in good agreement with the values found

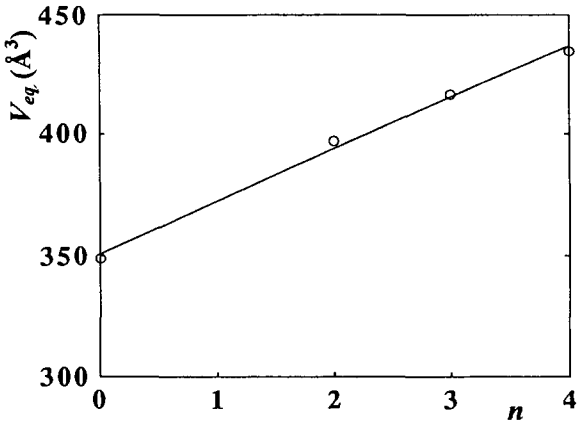

Fig. 11. Evolution of the chemical-unit-equivalent volume ($V_{eq} = V_{cell}/Z$) versus the number of water molecules n.

in the structure of $Ce(NO_3)_5(H_3O)_2.H_2O$ (mean value: 5.3 Å) [18].

Although a complete description of the structure of the crystalline compounds found in this study was not possible, it is worth noting that all patterns have been indexed, which indicates that the phases are pure. The relevance of the indexing solutions is clearly demonstrated by the linear variation of the chemical-formula-unit equivalent volume V_{eq} ($V_{eq} = V_{cell}/Z$) versus the number n of water molecules (Fig. 11). V_{eq} was calculated on the basis of $Z = 4$, except for the anhydrous phase ($Z = 8$). A similar variation of V_{eq} has already been found for the phases occurring in the thermal decomposition of $CeRb_2(NO_3)_5.4H_2O$ [5].

4. Conclusions

The new compound $Ce(NH_4)_2(NO_3)_5.4H_2O$ has been synthesized. It is isostructural with the related compounds $La(NH_4)_2(NO_3)_5.4H_2O$ and $CeRb_2(NO_3)_5.4H_2O$. The study of its thermal decomposition, by TDXD and TG–DSC, has revealed the intermediate cerium phases $Ce(NH_4)_2(NO_3)_5.3H_2O$, $Ce(NH_4)_2(NO_3)_5.2H_2O$, $Ce(NH_4)_2(NO_3)_5$, $Ce_2(NH_4)_3(NO_3)_9$, and amorphous NH_4NO_3. Their formation during the decomposition process is strongly dependent on the microstructure of the precursor and the reactional atmosphere. The formation of amorphous NH_4NO_3, together with $Ce_2(NH_4)_3(NO_3)_9$, during the dehydration of the trihydrated phase in nitrogen atmosphere, is an interesting feature of the decomposition. The presence of the amorphous phase is supported by the absence of Bragg reflections. It is an indication that the phase is non-crystalline, since even a nanocrystalline phase with very small crystallites (15–20 Å) should give visible broad diffraction lines. Additionally, the phase transformations characteristic of pure crystalline NH_4NO_3 [19] were not observed by DSC in the temperature range where the amorphous nitrate exists (45°–170°C). Then, it can be stated that, in a large temperature range, NH_4NO_3 is amorphous, in the sense that the atomic arrangements are not spatially periodic. It is the third example describing the formation of amorphous neutral nitrate during the thermal decomposition of mixed cerium nitrates. Indeed, the formation of amorphous $RbNO_3$ was clearly demonstrated, by DSC and TDXD, in the thermal decomposition of $CeRb_2(NO_3)_5.4H_2O$ [5] and $Ce_2Rb_3(NO_3)_9$ [3]. It is well known that metallic nitrates form disordered phases. A large variety of nitrate glasses have been reported [20,21] for single alkaline or ammonium nitrates,but not to our knowledge. Although in the present study amorphous NH_4NO_3 (and $RbNO_3$ in [3] and [5]) is not in a glassy state, the two physical distinct states (amorphous and glassy) are likely to be due to the trend of neutral nitrates to form disordered materials. On the other hand, it is not uncommon to observe amorphous phases during the thermal decomposition of crystalline materials, e.g. amorphous ZrO_2, preceding the crystallization of the tetragonal oxide, has been described during the thermal decomposition of crystalline zirconium hydroxide nitrates [22,23].

To conclude, the thermal decomposition scheme of $Ce(NH_4)_2(NO_3)_5.4H_2O$ has been described in detail. It is greatly complicated by the formation of amorphous NH_4NO_3. It is interesting to note that the anhydrous cerous nitrate and cerium oxide nitrate have not been observed in the present study, while the oxide nitrate has been identified for the related lanthanides La, Pr and Nd systems. TDXD has again been a powerful tool in the present investigation, however the use of DSC was essential to demonstrate the existence of amorphous ammonium nitrate.

Acknowledgements

Grateful thanks are expressed to the Conseil Régional de Bretagne for a support to one of the authors (NA) and G. Marsolier is acknowledged for his technical assistance.

References

[1] N. Audebrand, N. Guillou, J.P. Auffrédic and D. Louër, Thermochim. Acta, 286 (1996) 83.
[2] N. Guillou, J.P. Auffrédic and D. Louër, J. Solid State Chem., 15 (1995) 295.
[3] N. Guillou, J.P. Auffrédic and D. Louër, J. Solid State Chem., 122 (1996) 59.
[4] N. Guillou, J.P. Auffrédic and D. Louër, Acta Cryst., C51 (1995) 1032.
[5] N. Audebrand, J.P. Auffrédic, M. Louër, N. Guillou and D. Louër, Solid State Ionics, 84 (1996) 323.

[6] M. Leskelä and L. Niinistö, in K.A. Gschneidner Jr. and L. Eyring (Eds), Handbook of the Physics and Chemistry of the Rare Earths, Vol. 8, North-Holland, Amsterdam (1986), Chap. 56, p. 203.
[7] M. Karppinen, P. Kyläkoski, L. Niinistö and C. Rodellas, J. Thermal Anal., 35 (1989) 347.
[8] G. Meyer, E. Maneck and A. Reller, Z. Anorg. All. Chem., 591 (1990) 77.
[9] A. Boultif and D. Louër, J. Appl. Cryst., 24 (1991) 987.
[10] J. Plévert, J.P. Auffrédic, M. Louër and D. Louër, J. Mater. Sci., 24 (1989) 1913.
[11] M. Boll, in: Mémento du Chimiste I (Dunod, Paris, 1949).
[12] A.D. Mighell, C.R. Hubbard and J.K. Stalick, in: NBSAIDS80: a Fortran Program for Crystallographic Data Evaluation. NBS (US) Tech. Note 1141, 1981. (NBSAIDS83 is an expanded version of NBSAIDS80).
[13] International Centre for Diffraction Data, Philadelphia, PA.
[14] B. Eriksson, L.O. Larsson and L. Niinistö, Acta Chem. Scand., A36 (1982) 465.
[15] O. Knacke, O. Kubaschevski and K. Hesselmann (Eds.), Thermochemical Properties of Inorganic Substances, 2nd (edn.), Springer, Berlin (1991).
[16] J. Rodriguez-Carjaval, Collected Abstracts of Powder Diffraction Meeting, Toulouse, France (1990) p. 127.
[17] G.M. Sheldrick, Acta Cryst., A46 (1990) 467.
[18] N. Guillou, J.P. Auffrédic, M. Louër and D. Louër, J. Solid State Chem., 106 (1993) 295.
[19] J.S. Ingman, G.J. Kearley and S.F.A. Kettle, J. Chem. Soc., Faraday Trans. I, 78 (1982) 1817.
[20] L.G. van Uitert and W.H. Grodkiewicz, Mat. Res. Bull., 6 (1971) 283.
[21] D.W. James and M.T. Carrick, Aust. J. Chem., 39 (1986) 325.
[22] P. Bénard, J.P. Auffrédic and D. Louër, Powder Diffr., 8 (1993) 39.
[23] P. Bénard and D. Louër, J. Phys. Chem. Solids, 56 (1995) 1345.